water

MDPI

Article

Is There Spatial and Temporal Variability in the Response of Plant Canopy and Trunk Growth to Climate Change in a Typical River Basin of Arid Areas

Kaiye Yuan [1,2], Hailiang Xu [1,*] and Guangpeng Zhang [1]

[1] State Key Laboratory of Desert and Oasis Ecology, Xinjiang Institute of Ecology and Geography, Chinese Academy of Sciences, Urumqi 830011, China; yuanky2022@163.com (K.Y.); zgp@ms.xjb.ac.cn (G.Z.)
[2] University of Chinese Academy of Sciences, Beijing 100049, China
* Correspondence: xuhl@ms.xjb.ac.cn

Abstract: The response of plants to climate change has become a topical issue. However, there is no consensus on the synergistic processes of the canopy and trunk growth within different vegetation types, or on the consistency of the response of the canopy and trunk to climate change. This paper is based on Normalized Difference Vegetation Index (NDVI), tree-ring width index (TRW) and climate data from the Irtysh River basin, a sensitive area for climate change in Central Asia. Spatial statistical methods and correlation analysis were used to analyze the spatial and temporal trends of plants and climate, and to reveal the differences in the canopy and trunk response mechanisms to climate within different vegetation types. The results show a warming and humidifying trend between 1982 and 2015 in the study area, and NDVI and TRW increases in different vegetation type zones. On an interannual scale, temperature is the main driver of the canopy growth in alpine areas and precipitation is the main limiting factor for the canopy growth in lower altitude valley and desert areas. The degree of response of the trunk to climatic factors decreases with increasing altitude, and TRW is significantly correlated with mean annual temperature, precipitation and SPEI in desert areas. On a monthly scale, the earlier and longer growing season due to the accumulation of temperature and precipitation in the early spring and late autumn periods contributes to two highly significant trends of increase in the canopy from March to May and August to October. Climatic conditions during the growing season are the main limiting factor for the growth of the trunk, but there is considerable variation in the driving of the trunk in different vegetation type zones. The canopy growth is mainly influenced by climatic factors in the current month, while there is a 1–2-month lag effect in the response of the trunk to climatic factors. In addition, the synergy between the canopy and the trunk is gradually weakened with increasing altitude (correlation coefficient is 0.371 in alpine areas, 0.413 in valley areas and 0.583 in desert areas). These findings help to enrich the understanding of the response mechanisms to climate change in different vegetation type zones and provide a scientific basis for the development of climate change response measures in Central Asia.

Keywords: NDVI; tree-rings; canopy growth; climate change; arid region

check for updates

Citation: Yuan, K.; Xu, H.; Zhang, G. Is There Spatial and Temporal Variability in the Response of Plant Canopy and Trunk Growth to Climate Change in a Typical River Basin of Arid Areas. *Water* **2022**, *14*, 1573. https://doi.org/10.3390/w14101573

Academic Editor: Maria Mimikou

Received: 21 April 2022
Accepted: 12 May 2022
Published: 14 May 2022

Publisher's Note: MDPI stays neutral with regard to jurisdictional claims in published maps and institutional affiliations.

Copyright: © 2022 by the authors. Licensee MDPI, Basel, Switzerland. This article is an open access article distributed under the terms and conditions of the Creative Commons Attribution (CC BY) license (https://creativecommons.org/licenses/by/4.0/).

1. Introduction

Climate change poses a significant threat to ecosystem functions and services [1–3]. Maintaining and improving vegetation productivity is considered an important approach to mitigating and offsetting the adverse effects of climate change [4,5]. The dynamic patterns of plants productivity in response to climate change at global or regional scales have received widespread attention [6,7]. Climate change affects the physiological processes, distribution patterns, and productivity of plants by changing the fundamental processes of ecosystems (plant respiration, photosynthesis, water use efficiency, etc.) [8,9]. While, as the subject of terrestrial ecosystems, plants can also act as feedback to climate change directly

or indirectly by changing surface parameters (surface albedo, roughness, evapotranspiration, etc.) [10]. Accurate estimation and understanding of the interrelationship between plants productivity and climatic factors are crucial for clarifying the evolution of terrestrial ecosystems, determining ecosystem carbon sinks, and maintaining ecosystem functions.

It has been noted that the role of climate in regulating plants productivity varies according to the scale of study [11–13]. Plant growth is mainly influenced by temperature at mid to high latitudes in the Northern Hemisphere, while at regional scales it is more influenced by precipitation concluded that precipitation is the dominant driving factor of plants change [14], but precipitation has less influence on sub-humid areas and extremely arid areas [15]. Arid areas account for approximately 45% of the global land area [16], and their plant productivity plays an important role in the global carbon cycle [17,18]. In the context of continuing global climate change, dryland ecosystems are at risk of serious degradation [19,20]. Although previous studies have enriched our understanding of climate-plants response mechanisms, the complexity of the relationship necessitates an in-depth study of climate change patterns and plant response mechanisms in arid zones. In addition, much of our understanding of climate–plant relationships stems from studies at the individual, species-level of plants [21–23], while only a few scholars have comparatively analyzed the variability of plant organ responses to climate. Quantitative characterization of climate regulation of the canopy and trunk provides a direct and accurate picture of the nature and dynamics of ecosystem function. Plant leaves and trunks act as organs for the production and storage of organic matter, resulting in possible differences in the response of the growth processes to climate change due to the difference in growth cycle, organic matter storage capacity and form of existence of them [24,25]. In recent years, studies on the response of arbor canopies and trunks to climate change have brought different conclusions. Kannenberg et al. concluded that drought stress has a greater impact on tree-ring width (TRW) than Normalized Difference Vegetation Index (NDVI) in western US forests [26]. Chen et al. found that water promotes the trunk growth by mediating leaf photosynthesis [27]. In Central Asia, Wu et al. found consistency in the response of NDVI and RWI to temperature, but significant differences in their response to precipitation or PDSI [28].

Irtysh River Basin in China is an important channel for Arctic Ocean water vapor to enter Xinjiang, and a complete coupled Mountain–Plain–Desert ecosystem is developed in the region, hydro-ecological response processes to climate change are extremely sensitive and complex. In this study, the area was selected as the study area, and NDVI and TRW indices were selected to characterize the growth of plant canopies and trunks, respectively, and to explore how the canopy and trunk adjust their growth trends to adapt to climate change using temperature, precipitation, and SPEI data. How does the interaction of altitude gradient and climatic factors affect plant growth in alpine, plain and desert areas? Answering these questions will help us to further elucidate the plasticity of different vegetation zones in response to climate change.

2. Material and Methods

2.1. Study Regions

The study area is located within the basin of the Irtysh River (85°35′–90°30′ E, 46°52′–49°15′ N), an international river that originates in the Altai Mountains of China, flows through Kazakhstan and Russia, and eventually joins the Arctic Ocean. The study area has a temperate continental climate with long, cold winters and short, dry summers. A complex ecosystem has developed in the study area, which can be relatively divided into an alpine area, valley area, and desert area depending on the topography and vegetation (Figure 1). The altitude of the alpine area is from 1300 m to 3000 m, and the landscape is mountainous and a foreland with alpine meadows. The valley area is located in an alluvial fan plain with an altitude of 800 m to 1300 m, developed by riparian forests, low mountain meadows, and wetland swamps. The altitude of the desert area is from 400 m to 550 m and its vegetation type is mainly desert steppe.

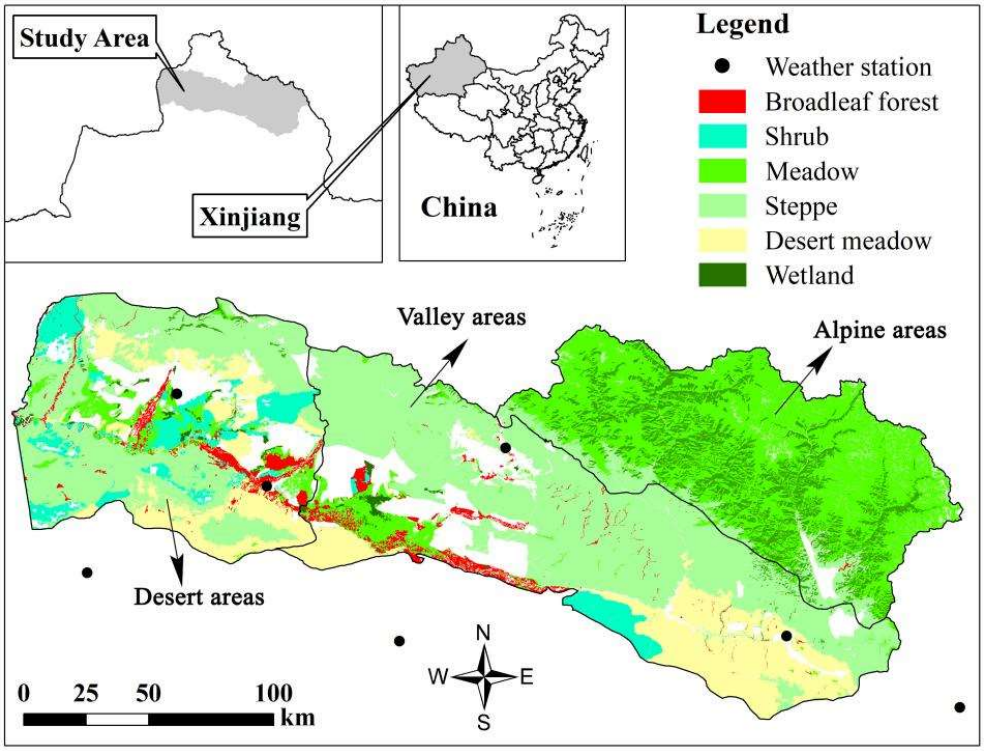

Figure 1. Geographical location of study area. According to the difference of the altitude, vegetation, the study area was divided into the alpine areas, valley areas and desert areas. The National Meteorological Stations are shown in the figure.

2.2. Sampling and Measurements

Meteorological data, including monthly temperature and precipitation from 1959 to 2015, were provided by the National Meteorological Information Center of China (http://data.cma.cn/ (accessed on 1 January 2020)). The MODIS NDVI data used in this research with a spatial resolution of 250 m and a temporal resolution of 16 days from 1982 to 2015 were obtained from the MOD13Q1 dataset released by NASA (https://ladsweb.modaps.eosdis.nasa.gov/ (accessed on 1 January 2020)). Savitzky–Golay filtering was applied to NDVI data processing to obtain higher quality data [29]. The maximum value composite (MVC) was processed for the 23 periods of each year to obtain the monthly NDVI representing the optimum growth of plants. Meanwhile, the cumulative value of NDVI from April to October (TINDVI) was used as an indicator representing the actual plants growth in a whole year. The total numbers of NDVI images selected were 782 images (46 images per year).

To minimize the impact of non-climatic factors on tree-ring width, sample trees that are less affected by human activity and far from rivers were prudently selected. At the breast height (1.3 m) of each healthy tree, two cores were obtained using a 5.15 mm diameter, drilled along the vertical slope and parallel slope directions. A total of 118 cores from 60 trees were sampled, respectively, 34 tree cores from 17 *Larix sibirica* (average height (aH) = 19 ± 0.32 m, average diameter at breast height (aDBH) = 1.3 ± 0.05 m) in the alpine area, 49 tree cores from 25 *Larix sibirica* (aH = 16 ± 0.2 m, aDBH = 1.6 ± 0.11 m) in the valley area, and 35 tree cores from 18 Betula platyphylla (aH = 18 ± 0.37 m, aDBH = 1.3 ± 0.09 m) in the desert area.

First, the sampled cores were pretreated with drying, fixation, and polishing. Then, the tree-ring width was measured with a LINTAB 6 measuring system coupled with the 'Time Series Analysis Programme' (TSAP) at an accuracy of 0.001 mm [30], and verified with COFECHA to strengthen the cross-matching between trees [31]. By using the "Arstan" program, a negative exponential function was chosen to fit the growth trend. The age-related radial growth pattern raw tree-ring series and a chronology was created [32]. Higher

values of total sample interpretation for the standard chronology of the tree-ring width (STD). For this reason, a standard chronology of trees was selected for comparative feature analysis. The statistical characteristics of chronology indicate that the samples used in this paper are sufficiently representative and suitable for the chronoclimatological study (mean sensitivity, MS) (MS) > 0.2 [33], expressed population signal (EPS) > 0.75) (Table 1).

Table 1. Standard chronology characteristics of sampling the tree-ring.

Area	Time Series	MS	SD	SNR	EPS	AC1	MC
Alpine	1959–2015	0.284	0.466	3.308	0.768	0.449	0.500
Valley	1959–2015	0.281	0.222	7.314	0.88	−0.201	0.556
Desert	1959–2015	0.282	0.236	10.234	0.911	0.176	0.65

Note: MS, expressed mean sensitivity. SD, expressed standard deviation. SNR, expressed the signal-to-noise ratio. EPS, expressed population signal. AC1, expressed first-order autocorrelation coefficient. MC, expressed all sample cores correlation coefficient.

2.3. Data Analysis

2.3.1. SPEI

Standardized Precipitation Evapotranspiration Index (SPEI), not only considers the water and energy balance process, but also reflects the surface water deficit and accumulation process [34]. The SPEI can be calculated with multiple time scales (1, 3, 6, 12, 24, 48 months, etc.), the 1-month scale and the 12-month scale SPEI was used in this study to reflect the monthly and the interannual drought, respectively. The calculation procedures are as follows:

The Thornthwaite method was used to calculate the monthly potential evaporation (*PET*) [35]:

$$PET = 16K\left(\frac{10T}{I}\right)^{m} \quad (1)$$

In the formula, K is the correction factor based on the latitude, T is the monthly average temperature, I is the total annual heating index, m is the coefficient determined by I.

Calculation of the difference *(D)* between month-by-month precipitation and potential evapotranspiration:

$$D_i = P_i - PET_i \quad (2)$$

In the formula, P_i is the monthly precipitation and PET_i is the monthly potential evapotranspiration.

A log-logistic distribution was fitted to D_i and a cumulative function was derived:

$$f(x) = \frac{\beta}{\alpha}\left(\frac{x-\gamma}{\alpha}\right)^{\beta-1}\left[1+\left(\frac{x-\gamma}{\alpha}\right)^{\beta}\right]^{-2} \quad (3)$$

$$F(x) = \int_0^x f(t)dt = \left[1+\left(\frac{\alpha}{x-\gamma}\right)^{\beta}\right]^{-1} \quad (4)$$

In the formula: α is the scale parameter, β is the shape parameter, γ is the origin parameter, *f(x)* is the probability density function, $F(x)$ is the probability distribution function.

The sequences are normalized and normalized to obtain the corresponding SPEI:

$$\mathrm{SPEI} = W - \frac{C_0 + C_1 + C_2W^2}{1 + d_1W + d_2W + d_3W} \quad (5)$$

$$W = \sqrt{-2\ln p} \quad (6)$$

In the formula: when $p \leq 0.5$, $p = F(x)$; when $p > 0.5$, $p = 1 - F(x)$. The other parameters are C_0 = 2.515517, C_1 = 0.802853, C_2 = 0.010328, d_1 = 1.432788, d_2 = 0.001308.

2.3.2. Mann–Kendall Test

The Mann–Kendall statistical test was used to analyze the trends of climate and plants growth (climate indicators: temperature, precipitation, SPEI; plants growth: TRW index, monthly NDVI and TINDVI) in the alpine, valley and desert areas respectively. The Mann–Kendall statistical test is a non-distribution test in which the data do not need to be in a particular order and are not affected by outliers [36,37]. The time series of all indicators used for the Mann–Kendall test are uniform from 1982 to 2015. For the sequence of climatic and ecological indicators $X_i = (X_1, X_2, X_3,...,X_n)$, and the results are recorded as $sgn(\theta)$:

$$sgn = \begin{cases} 1 & \theta > 0 \\ 0 & \theta = 0 \\ -1 & \theta < 0 \end{cases} \quad (7)$$

The Mann–Kendall statistics are calculated as:

$$s = \sum_{i=1}^{n} \sum_{k=i+1}^{n} sgn(x_k - x_i) \quad (8)$$

X_k and X_i are consecutive data values, n is the length of the dataset.

The test statistic Zc is calculated as follows:

$$Z_c = \begin{cases} \frac{s-1}{\sqrt{\mathrm{var}(s)}}, & s > 0 \\ 0, & s = 0 \\ \frac{s+1}{\sqrt{\mathrm{var}(s)}}, & s < 0 \end{cases} \quad (9)$$

In the formula, $|Z_c| \geq 1.96$ and $|Z_c| \geq 2.58$ indicates that sequences showed significant trend changes at $p< 0.05$ and $p < 0.01$. $Z_c > 0$ indicates an upward trend, $Z_c < 0$ indicates a downward trend.

Commonly, β representing the change rate of time series, is calculated as follows [38,39]:

$$\beta = Median\left(\frac{x_i - x_k}{i - k}\right), \qquad \forall < 1 < j < i < n \quad (10)$$

In the formula, $\beta > 0$ indicates that the tested data shows an upward trend, and $\beta < 0$ indicates that the tested data shows a downward trend.

2.3.3. Mutation Test

The mutation of annual temperature, annual precipitation, and 12-month scale SPEI, TRW index, and TINDVI were analyzed by using the mutation test. The mutation test has been widely used to elucidate trends in hydrological, climatic, and environmental factors [40]. To perform the mutation test, a rank sequence (Sk) for time series should be constructed:

$$S_k = \sum_{i=1}^{k} \sum_{j}^{i-1} \alpha_{ij}, \ \mathrm{k} = 2,\ 3,\ 4, ..., \mathrm{n} \quad (11)$$

$$\alpha_{ij} = \begin{cases} 1 & x_i > x_j \\ 0 & x_i < x_j \end{cases}, \ \mathrm{j} = 1,\ 2, ..., \mathrm{i} \quad (12)$$

The statistic UF_k is defined as:

$$UF_k = \frac{[S_k - E(S_k)]}{\sqrt{V_{ar}(S_k)}}, \ \mathrm{k} = 2,\ 3,\ 4, ..., \mathrm{n} \quad (13)$$

In the formula: $E(S_k)$ is the mean value of Sk; $\sqrt{V_{ar}(S_k)}$ is the contrast of Sk; UF_k is the standard normal distribution, the result of $|UF_K| < \mu_{0.05}$ represents that the series has a significant trend during this period. If the two curves of UF and UB intersect at the critical

point, the moment corresponding to the intersection point is the time when the abrupt transition begins.

2.3.4. Contribution of Monthly NDVI Variation to TINDVI Variation

Based on the results of the Mann–Kendall test, a method for calculating the contribution rate of monthly NDVI variation to TINDVI variation was developed. The Z_C of NDVI (April to October) and TINDVI were used to calculate the p value with the standard normal distribution curve ($\varphi(t)$~$N(0, 1)$).

$$P(X = Z_C) = 1 - 2(1 - P(X \leq Z_C)) \tag{14}$$

$$P(X \leq Z_C) = \int_{-\infty}^{|Z_C|} \varphi(t)dt \tag{15}$$

In the formula, $P(X = Z_C)$ is the probability of occurrence of test statistic Z_C value. $P(X \leq Z_C)$ is the probability value of one-side estimation.

Further, the p value also is the probability of occurrence of β value, which makes the following equation true:

$$\beta_{TINDVI} \bullet P(X \leq Z_C)_{TINDVI} = \sum_{i}^{n} (\beta_{NDVI} \bullet P(X \leq Z_C)_{NDVI}) \tag{16}$$

Thus, the formula of contribution rate is as follows:

$$C = (\beta_{NDVI} \bullet P_{NDVI}) / (\beta_{TINDVI} \bullet P_{TINDVI}) \times 100\% \tag{17}$$

In the formula, β_{TINDVI} and β_{NDVI} were the annual variation of TINDVI and NDVI. The C is the contribution rate of monthly NDVI variation to TINDVI variation.

3. Results

3.1. Climate Change

The increasing trend of temperature in the study area gradually decreases with decreasing elevation. The annual temperature in the alpine, valley areas showed a significant increasing trend ($Z > 1.96$) (Table 2), with the increasing rates of 0.51 °C/10a and 0.35 °C/10a, respectively. Whereas, in the desert region, it showed a non-significant increasing trend ($0 < Z < 1.96$). Analogously, the annual precipitation in the alpine region increased significantly at the rate of 3.12 mm/a, but the annual precipitation in valley and desert areas increased insignificantly ($0 < Z < 1.96$) at the rate of 0.86 mm/a and 1.16 mm/a, respectively. Entirely, the SPEI in alpine, valley and desert areas showed non-significant increasing trends ($0 < Z < 1.96$), at rates of 0.82×10^{-2}/a, 1.55×10^{-2}/a, and 2.64×10^{-2}/a, respectively, indicating that the study area was being meteorologically humidified.

Table 2. Characteristics of interannual variation of climatic indicators.

Area	Factor	*Z*-Value	*β*-Value	Variation Tendency	Mutation Year
Alpine	Temperature	2.36	0.052 °C/a	*	NS
	Precipitation	2.42	3.12 mm/a	*	NS
	SPEI	0.52	0.0082/a	NS	1996
Valley	Temperature	1.97	0.017 °C/a	*	NS
	Precipitation	1.02	1.16 mm/a	NS	NS
	SPEI	0.79	−0.016/a	NS	1996
Desert	Temperature	1.32	0.035 °C/a	NS	NS
	Precipitation	1.11	1.16 mm/a	NS	NS
	SPEI	1.47	−0.026/a	NS	1996

Note: * for $p < 0.05$ significant level test, NS for $p > 0.05$ significant level test.

Figure 2 shows that on a monthly scale, temperatures within the basin show a trend of increasing from January to March and decreasing from May to July. Moreover, the increasing trend in the desert area reached a significant level ($1.96 < Z < 2.58$) from January to March and from May to July, and that in the alpine areas reached significant increase level in April and August ($1.96 < Z < 2.58$). Except for September, precipitation across the basin tended to increase from March to November and reached significant levels in April ($1.96 < Z < 2.58$), and an extremely significant level ($Z > 2.58$) from June to July. Then precipitation tended to decrease from December to February of the following year. The SPEI shows an arid meteorological trend in the basin between March and May and October ($1.96 < Z < 2.58$; $Z > 2.58$) and a meteorological trend of humidification between June and September and November and December.

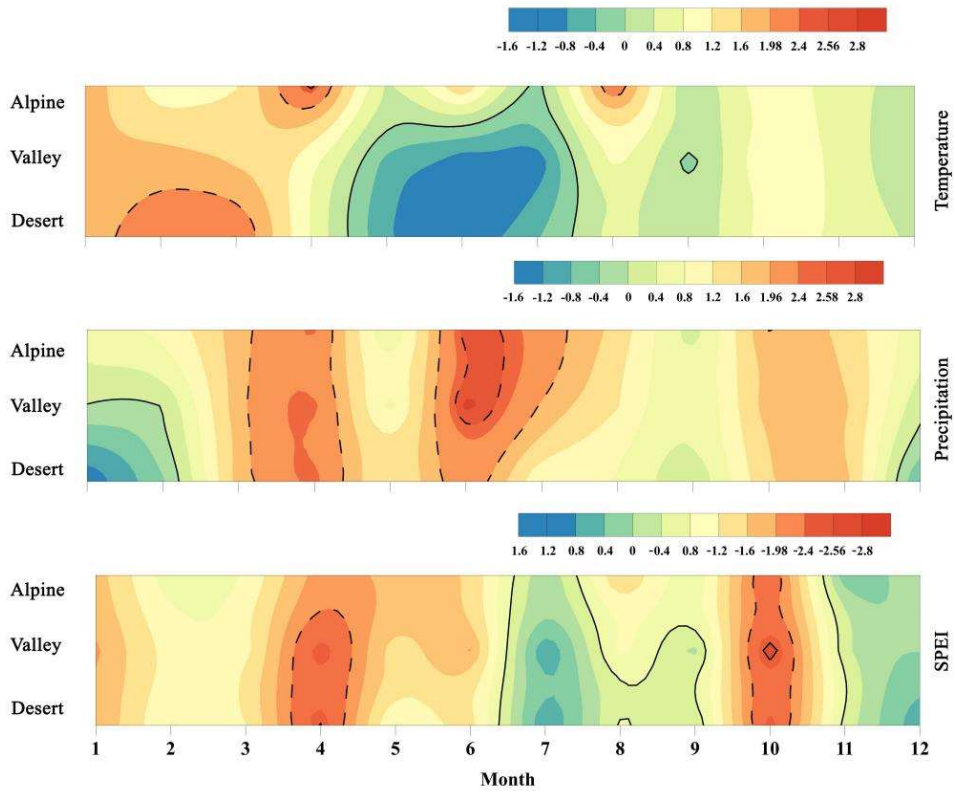

Figure 2. Trend test results of monthly temperature, precipitation, and SPEI. Note: the solid line is the border of the time horizon indicating an increasing ($Z_C > 0$) and decreasing ($Z_C < 0$) trend. Further, the dotted line is the border of the time horizon representing the significant increase ($Z_C > 1.96$, $p < 0.05$) (including the extremely significant increasing trend ($Z_C > 2.58$, $p < 0.01$)) and the non-significant increasing trend ($|Z_C| < 1.96$, $p < 0.05$).

3.2. Spatio-Temporal Variation of TINDVI and NDVI

Results of the TINDVI's trend test (Figure 3) showed an extremely significant increasing trend ($Z > 2.58$) at rates of 10.2×10^{-3}/a and 4.5×10^{-3}/a in alpine and desert areas, and a significant increasing trend at a rate of 4.3×10^{-3}/a in the valley area ($1.96 < Z < 2.58$). The results of the TINDVI's trend test at the pixel scale indicated that the proportion of pixels increasing and decreasing were 80.3% and 19.7% (Figure 4). Specifically, there was 94.02%, 73.18% and 74.32% of the pixel in alpine, valley and desert areas, respectively, showing an increasing trend. Furthermore, the proportion of pixels showing a significant increasing trend ($Z > 1.96$) were 71.09%, 32.93% and 48.6%, respectively.

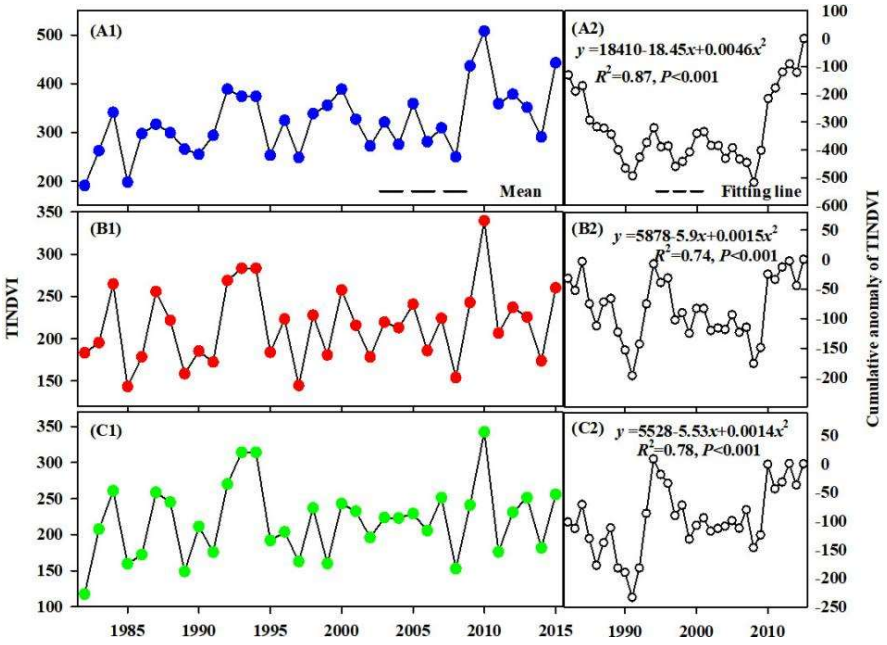

Figure 3. Interannual variation characteristics of TINDVI. (**A1**,**B1**,**C1**) show the annual change of TINDVI in alpine, valley and desert. Meanwhile, (**A2**,**B2**,**C2**) show the change of cumulative anomaly of TINDVI in alpine, valley and desert. The fitting line of the cumulative anomaly of TINDVI indicated that there was a significant increasing mutation in the alpine, valley and desert areas. The line of mean value showed a variation of TINDVI after mutation occurred.

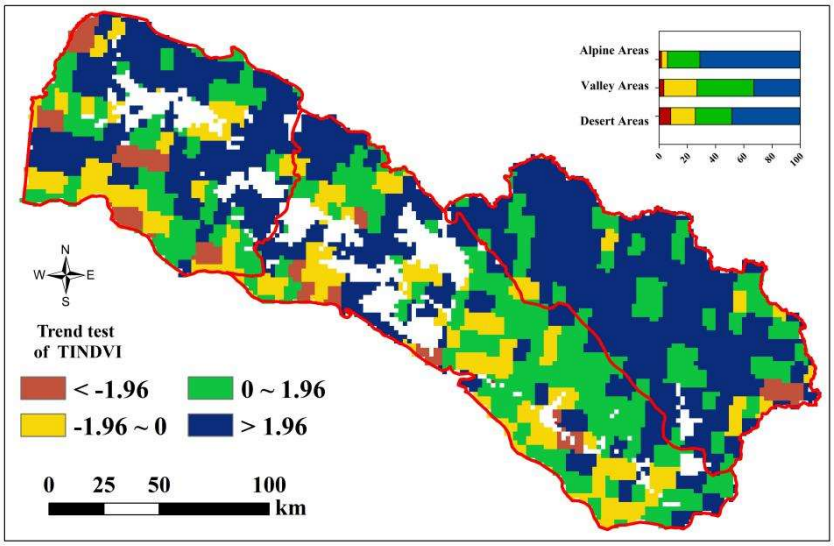

Figure 4. Spatial distribution of trend test value of TINDVI. Note: The histogram in the plot showed the proportion of areas with significant ($|Z_C| > 1.96$, $p < 0.05$) and non-significant ($|Z_C| < 1.96$, $p < 0.01$) changes.

The results of the trend test of monthly NDVI showed that there were two "hot zones" and one "cold zone" during the growth season, definitely (Figure 5). One of the "hot zones" occurred from March to May in the basin. Particularly, from mid-March to mid-April, a "hot zone" with an extremely significant increasing trend ($Z > 2.58$) in the valley and desert regions was exhibited. Meanwhile, from August to October, another "hot zone" with a significant increasing trend ($1.96 < Z < 2.58$) appeared, which became progressively narrower (i.e., the duration of the significant increase in NDVI became shorter) from desert to alpine areas, and the beginning time when NDVI increased significantly was accompanied by hysteresis (desert: August, valley: September, mountainous areas: mid-

September). The "cold zones", showing significant decreases ($Z < -1.96$), were mainly concentrated in alpine areas in August, and in the valley and desert areas in June and July, while NDVI in alpine areas still increased. Further, the increasing trend of NDVI continued into November. The above showed that the plant growth in the study area was more vigorous during the advanced re-greening and late growing season, but was suppressed obviously during the peak growth period, and the growing season duration increased.

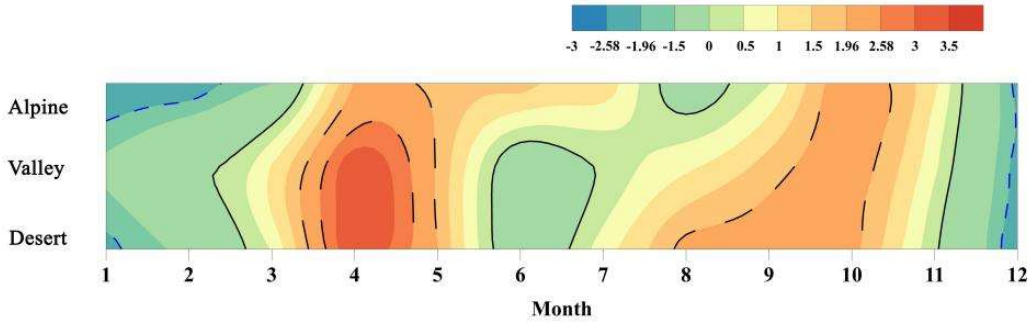

Figure 5. Trend test results of monthly NDVI. Note: the solid line is the border of the time horizon indicating an increasing ($Z_C > 0$) and decreasing ($Z_C < 0$) trend. Further, the dotted line is the border of the time horizon representing the significant increase ($Z_C > 1.96$, $p < 0.05$) (including the extremely significant increasing trend ($Z_C > 2.58$, $p < 0.01$)) and the non-significant increasing trend ($|Z_C| < 1.96$, $p < 0.05$).

3.3. Change in TRW

Entirely, the results of the trend test of TRW index in the alpine, valley, and desert areas, showed a non-significant increasing trend (Figure 6A1,B1,C1). Furthermore, the standard chronology increased at the rates (β) of 1.32×10^{-3}/a, 1.1×10^{-3}/a, and 1.06×10^{-3}/a, respectively. As shown in Figure 6A2,B2,C2, the variation of a cumulative anomaly of the TRW index did not conform to the apparent "single valley" process. Further, the transition time obtained by mutation test of TRW index was not completely consistent with the results of cumulative anomaly, indicating that there is no mutation for tree-ring growth in Irtysh River Basin.

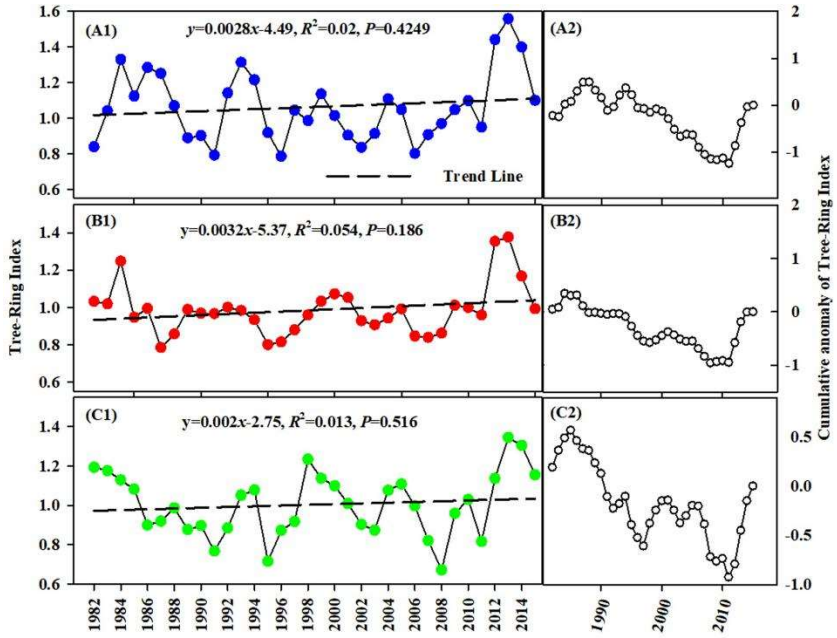

Figure 6. Interannual variation characteristics of TRW. Note: (**A1**,**B1**,**C1**) show the annual change of TRW in alpine, valley and desert areas. Meanwhile, (**A2**,**B2**,**C2**) show the change of cumulative anomaly of TRW in alpine, valley and desert areas.

4. Discussion

4.1. Influence of Climate Change on NDVI

Due to the uneven distribution of heat and moisture, the vegetation types within the Irtysh River basin are broadly alpine meadow–broadleaf forest–desert vegetation from upstream to downstream. This study found that climate was the main, but not the only, factor controlling vegetation patterns, as plant responses to climatic factors varied with altitude (Table 2 and Figure 3). The results of the Pearson test (Figure 7), showed that TINDVI in alpine areas was significantly positively correlated with temperature and negatively correlated with SPEI (Figure 7B,C,E,F). TINDVI was positively but not significantly correlated with climatic factors in both the valley and desert areas. The relationship between plant growth and climatic factors shifted as altitude decreased. No significant correlation was found between TINDVI and meteorological elements in both plains and desert areas.

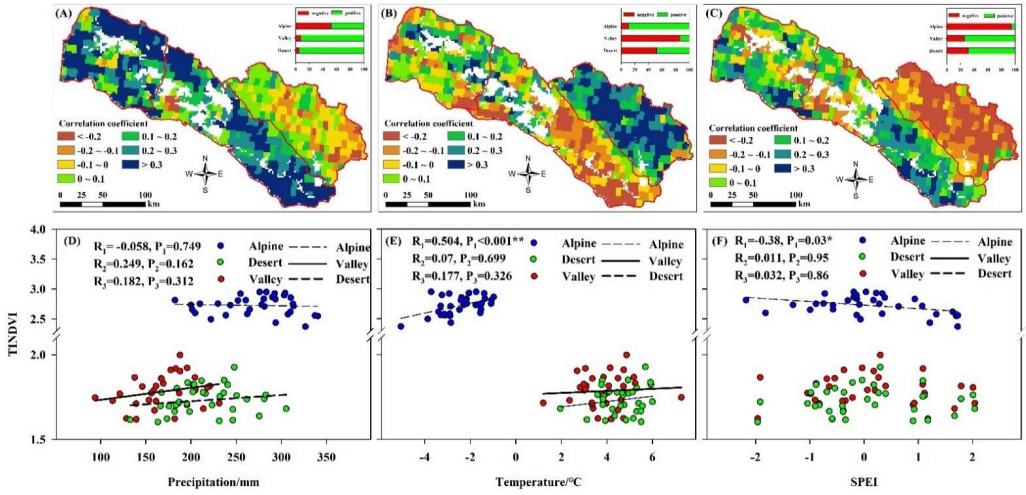

Figure 7. Correlation between precipitation, temperature and SPEI and TINDVI. Note: (**A**–**C**) show the spatial distribution of correlation coefficient between precipitation, temperature and SPEI and TINDVI. Further, the histogram in (**A**–**C**) show the proportion of positive and negative correlations. (**D**–**F**) show the temporal correlation between annual precipitation, annual temperature and annual SPEI and annual average of TINDVI. R_1, R_2 and R_3 value in alpine, valley and desert are shown in each plot. So is the p value. * $p < 0.05$, ** $p < 0.01$.

The trend changes of NDVI and meteorological factors on the monthly scale (Figures 3 and 5) found that the increase of NDVI in the Irtysh River basin on the time series was mainly due to the advancement of the growing season and the extension of the growing period. The results validate the physiographic view that the positive correlation between plant productivity and growing season duration [41,42]. Furthermore, it is interesting that the growth peak of NDVI in the whole watershed occurs in spring and autumn rather than summer, from March to May, NDVI growth reached its first peak ($p < 0.05$) i.e., the re-greening stage of plants, during the same period, where precipitation showed a significant increasing trend ($p < 0.05$), and the temperature from January to March showed a significant increasing trend ($p < 0.05$), which indicates that moisture and temperature in early spring are the dominant climatic factors in plant re-greening period in the study area. The accumulation of temperature in the early stage and the increase of available water is beneficial to breaking dormancy, stimulating cell division, improving photosynthetic efficiency and carbohydrate accumulation, and providing sufficient energy for plant growth; this is consistent with the results of previous studies in arid regions [43,44]. Instead, during the critical period of plants growth and development, May to August, NDVI tends to decrease throughout the watershed, this period, there was a significant downward trend in temperature ($p < 0.05$), precipitation showed a significant increase ($p < 0.05$), SPEI changed

from drought to wetness; this indicates that summer drought and low temperatures limit plant growth. Due to the influence of spring warming, plant phenology was advanced and plant productivity increased, but the earlier start of plant transpiration reduced available water. Even if the precipitation increases in summer, the whole basin is still dry. The research of Lian et al. in the Northern Hemisphere also showed that the increment of precipitation was not enough to compensate for the transpiration of plants in spring, and that the drought trend would continue through the summer [45]. In addition, the increase in precipitation leads to an increase in cloudiness and a decrease in insolation duration and solar radiation [46,47], resulting in a decrease in temperature and a decrease in plant photosynthesis, which inhibits the growth of plants. At the termination of the growing season from August to October, the NDVI of the whole basin showed a second increasing trend, and although the temperature and precipitation showed a decreasing trend during the same period, the SPEI showed a shift from wetting to a dry trend in October (October, $p < 0.01$). This indicates that autumn is relatively humid and temperatures increase in late autumn. Suitable hydrothermal conditions and high temperatures at the end of autumn extend the growth period and promote the growth of plants. This is consistent with the results of Gao et al.: climate warming leads to the delay of global autumn phenology [48]. On the one hand, the rising temperature in late autumn ensures photosynthesis is still active at the terminal stage of the growing season, which is conducive to the accumulation of photosynthetic products and provides sufficient nutrients for plant growth [49,50]; on the other hand, the increase of precipitation and SPEI in autumn increased the amount of water available to plants, driving the rate of carbohydrate conversion into plant cells and organs. Jeong et al. concluded that the extension of the plant-growth period in the Northern Hemisphere is mainly influenced by autumn temperatures [51].

In terms of spatial sequence, this study found that NDVI had different responses to climate along the altitude gradient. Altitude, as an important ecological factor affecting plant growth, causes the plant growth environment to become more complex by changing biotic and abiotic elements, and thus plant activities are different [52–55]. Between August and October, the increasing trend of NDVI decreases with an increase in altitude. It is noteworthy that with the increase in altitude, the decreasing trend of temperature is weakened; SPEI showed a trend of drought. This indicates that the higher the increase in altitude during this period, the more detrimental it is to the increase of NDVI. Previous studies have shown that the length of plants growth period is significantly shortened with the increase in altitude [56,57]. Warming at high-altitude areas aggravates the moisture stress of plants and slows down the growth of plants [58,59]. In addition, this study found that the lagging effect of plants became more pronounced with increasing altitude. The lagging effect is mainly because temperature and precipitation affect the effective accumulated temperature and available water to regulate the cycle of photosynthesis, respiration and soil nutrients, which in turn affects plant growth [60,61]. The temperature in the study area decreases with the increase in altitude. As the low temperature will reduce the mineralization rate of soil organic matter [62] and hinder the accumulated temperature conditions required for plants growth. Therefore, the plants growth in the alpine area takes a longer time to accumulate and shows a lag.

4.2. Effect of Climate Change on Tree-Ring Width

At the interannual level, there was no significant correlation between TRW and climatic factors in alpine and valley areas and the correlation between TRW and meteorological factors in the desert area reached a significant level (Figure 8). This also validates the previous study that with the increase in altitude, the sensitivity of trees to climate showed a downward trend [63–65]. This may be related to tree physiological activity and regional characteristics, Qiang et al. found that with the increase in altitude, trees reduce the level of physiological metabolism by controlling the stomatal density and dry weight of leaves to avoid the impact of climate change to the maximum extent [66]. In addition, the geography of the alpine and valley areas is more complex compared to the desert areas,

the relationship between tree growth and climate variables is more susceptible to other factors. In contrast, desert areas with poor soils and fragile ecology are extremely sensitive to climate change [19,20].

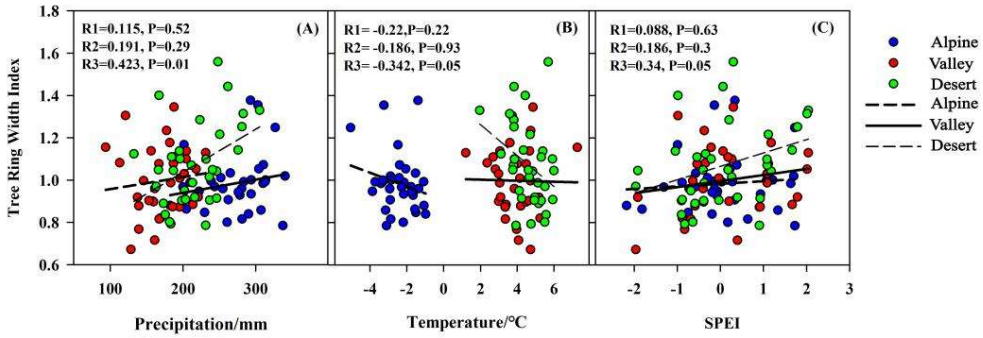

Figure 8. Correlation between TRW and climatic factors. Note: R1, R2 and R3 values in alpine, valley and desert areas are shown in each plot. So is the *p* value.

By analyzing the monthly data of TRW and meteorological factors, in this study, the strongest correlation between TRW and climatic factors during the growing season was found in the Irtysh River basin, this is consistent with the view of Seftigen et al. [67]. The precipitation, temperature and SPEI in the growing season of alpine and valley areas can promote TRW. TRW in the alpine area has a significant positive correlation with April precipitation and temperature in July ($p < 0.05$). *Larix sibirica* in the alpine area gradually enters the growth period in April, and it mainly depends on water in the early growth stage of xylem cambium cell differentiation [68,69]. During this period, the increase of precipitation can promote the radial growth of trees. In July, the *Larix sibirica* entered the peak period of growth, higher temperatures facilitate photosynthesis in plants, increasing cell productivity and forming wider tree-rings [70]. On the contrary, low temperature will reduce the photosynthetic efficiency of plants, cold air will even freeze to death the young branches and leaves that are just beginning to grow, thus forming narrow rings. Zhou et al. also found on the southern slopes of the Altai Mountains in China (surrounding our study area) that summer temperatures of the current year had a positive effect on the radial growth of *Larix sibirica* in the alpine area [71]. This was also verified by Churakova et al. in the Siberian areas (surrounding our study area) [72]. The results of this study have been found in other high-altitude areas [73].

TRW in the valley area was significantly and positively correlated with the temperature at the beginning of the growing season (April to June) ($p < 0.05$). In May, water vapor from the Caspian Sea and the Mediterranean Sea is constantly transported to the valley area by southwesterly air currents [74]. Under conditions of sufficient moisture, the increase of air temperature at the beginning of the growing season is beneficial to quickly reach the accumulated temperature requirement for tree growth, stimulate the cell division of cambium, and increase the width of earlywood. However, from June to August, the positive effect of temperature on the radial growth of *Larix sibirica* in the valley area gradually diminished and showed a significant positive correlation with precipitation ($p < 0.05$). This is due to the higher temperatures in the valley area from June to August, when water is dissipated from the soil and plants by transpiration, and tree growth is stressed by available water. In addition, the stomatal closure of leaves due to increased saturated water vapor pressure deficit in the forest floor leads to the phenomenon of photosynthetic lunch break [75], which inhibits the radial growth of trees and thus produces narrow whorls. Therefore, the radial growth of trees in the valley area was significantly and positively correlated with summer precipitation. This is in agreement with the results of other studies on *Larix sibirica* [76,77].

With a decrease in altitude, the positive effect of temperature on tree growth, changes to an inhibitory effect on TRW in desert areas. In this study, we found that TRW in the desert

area was significantly and positively correlated with SPEI in February, and the correlation coefficient with precipitation reached 0.8. The radial growth of trees in the desert area in February was mainly influenced by moisture, the negative correlation between TRW and the temperature in February also proves this point. This means that the climate during the dormant season has an important influence on the radial growth of trees [78]. In the arid and rainless desert area, water is scarce in February, rising temperature causes the increased respiration of the trees, exacerbating the consumption of stored nonstructural carbohydrates. Thus, radial growth is inhibited. In addition, during this period the leaves have not yet unfolded; the photosynthetic capacity of the leaves is weak and the tree is at risk of carbon starvation. Furthermore, the increase in temperature in February shortens the time of bud dormancy and reduces the resistance of trees to cold waves [79,80]. This conclusion is similar to the findings of Jiang et al. in the central Altai Mountains (surrounding our study area) [81]. From May to June at the beginning of the growing season, TRW was highly significantly negatively correlated with temperature ($p < 0.01$), and highly significant positive correlation with May SPEI ($p < 0.01$), and the correlation coefficient with precipitation reached 0.9. This indicates that trees in the desert area are still under moisture stress during the rapid-growth stage. Currently, the desert area is well-heated, where temperature affects photosynthesis in trees by regulating respiration, transpiration and gas exchange. High temperature is beneficial to the respiration of trees but not to the accumulation of nonstructural carbohydrates [82], where the deficit of available water leads to slow radial growth. This also verifies the previous view that tree growth in arid regions is mainly influenced by precipitation [68].

4.3. Relationship between Plant Canopies and Trunks

On an interannual scale (Table 3), NDVI and TRW are positively correlated in the Irtysh River basin, and similar results have been obtained in other regions [83–85]. The correlation between NDVI and TRW has a clear physiological basis, NDVI is an index synthesized from the reflectance values of plant reflectance spectral curves and reflects mainly the greenness of plant leaves and canopy growth [86–89]; TRW characterizes the amount of radial growth of a tree, the growth rate of which is related to the net material accumulation of the plant after photosynthesis minus respiration [90,91]; while the leaves are the main organ of photosynthesis and their growth condition determines the amount of material required for radial growth, therefore, there is a correlation between the plant canopy and the trunk [25,92]. In addition, the correlation between TRW and NDVI in the Irtysh River basin decreases with increasing elevation, with correlation coefficients of 0.371 in high mountainous areas, 0.413 in valley areas and 0.583 in desert areas. The Irtysh River basin is located in an arid zone where climatic conditions of scarce precipitation and high temperatures have a strong disturbing effect on plant growth, while with increasing elevation, precipitation increases, temperature decreases, severe climatic constraints are alleviated, vegetation cover increases, and NDVI shows a significant lagging effect with increasing basin elevation (Figure 5), which in turn reduces the degree of correlation with TRW.

In addition, this study found that the lagged effect of TRW on meteorological factors was greater than that of NDVI (Figure 9), which also verified the temporal heterogeneity of carbon uptake and storage [93–95]. This is shown by the fact that NDVI correlates best with the meteorological factors of the month in the basin, while TRW correlates best with the meteorology of the previous 1–2 months. On the one hand, plants have a dynamic carbon allocation strategy for climate response, preferentially allocated to the canopy rather than the trunk, resulting in a longer lag effect of TRW than NDVI [96]. On the other hand, trunk growth is associated with long-term carbohydrate accumulation and requires a certain cycle from wood cell development to lignification [83,97–99]. Detailed information on the relationship between NDVI and TRW can be gathered from the monthly values, with the best correlation between NDVI and TRW for the whole basin during the growing season period (Table 3). The highest correlation between TRW and July NDVI was found

throughout the basin (Figure 10), with significant correlations between TRW and July NDVI in the valley and desert regions (R2 = 0.96, $p < 0.01$; R2 = 0.99, $p < 0.05$). This also validates previous findings in the Northern Hemisphere that tree annual ring width is highly correlated with July NDVI [24,100], with trees completing major cell division and expansion around July, followed by a phase of cell wall thickening with less variation [101], during which good hydrothermal conditions also promote plants in the watershed. The canopy reaches its maximum value for the year during this period, resulting in the best correlation between annual tree-ring width and NDVI in July.

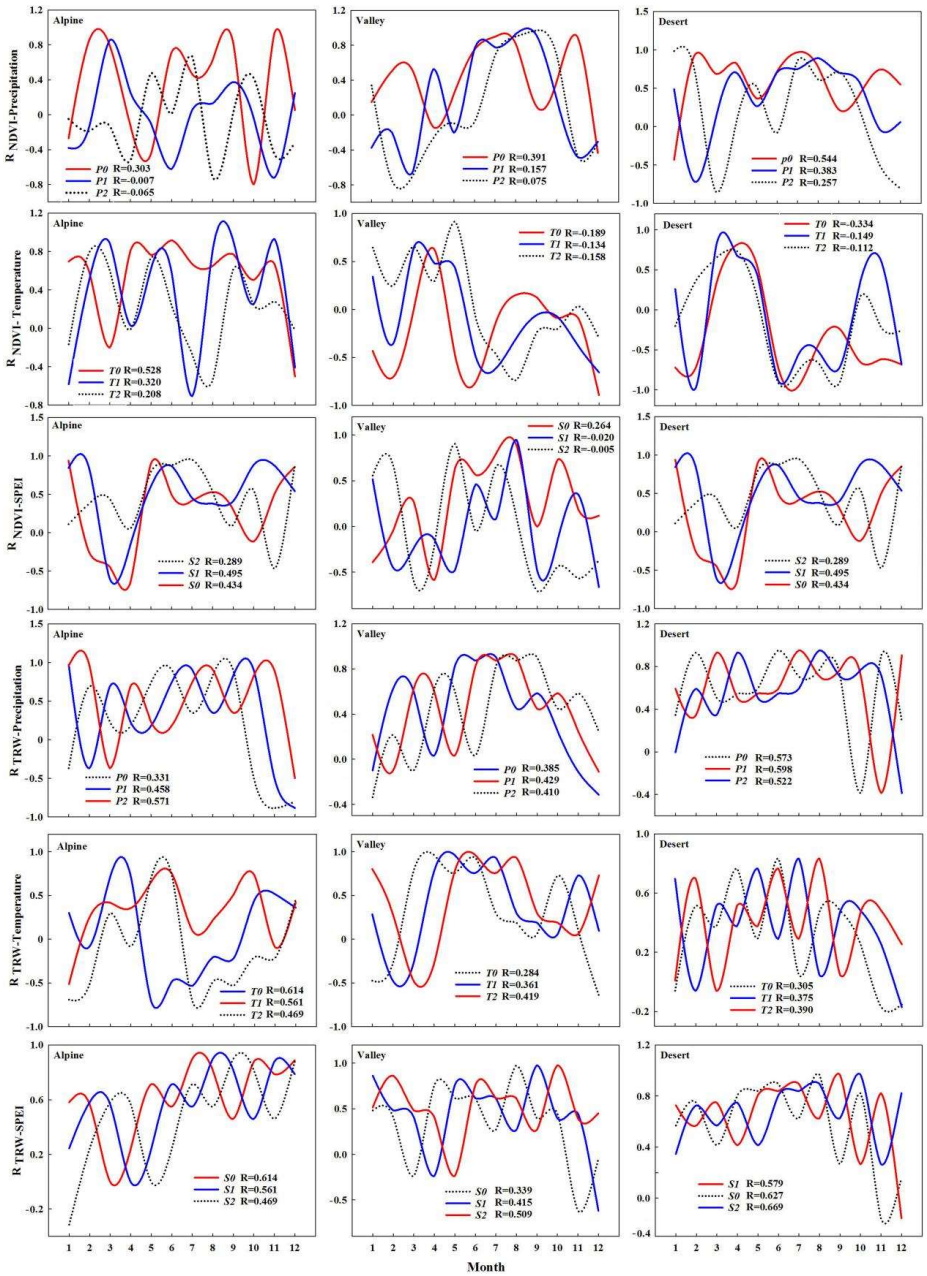

Figure 9. Hysteresis effects of NDVI, TRW on climate factors. Note: *T0*, *T1* and *T2* represent the temperature of the current month, the temperature of the previous month and the temperature of the previous 2 months, respectively. *P0*, *P1* and *P2* indicate the precipitation of the current month, the precipitation of the previous month and the precipitation of the previous 2 months, respectively. *S0*, *S1* and *S2* indicate the SPEI of the current month, the SPEI of the previous month and the SPEI of the previous 2 months, respectively.

Table 3. Correlation between TRW and NDVI. Note: * $p < 0.05$.

NDVI	TRW of Alpine Areas	TRW of Valley Areas	TRW of Desert Areas
The interannual level	0.413	0.413	0.413
Pre-growing season (January to March)	0.495	0.638	0.684
Growing season (April to August)	0.827	0.852 *	0.903 *
Late growing season (September to December)	0.014	0.507	0.332

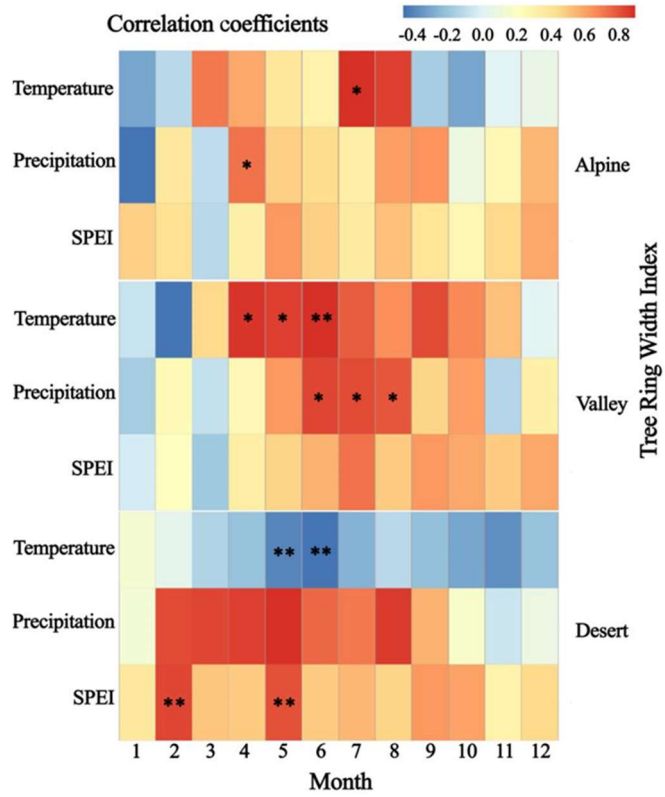

Figure 10. Correlation analysis of TRW index and monthly climatic factors. Note: * $p < 0.05$, ** $p < 0.01$.

5. Conclusions

A study, based on the spatial and temporal differences in the response of the canopy and trunk to climate in different vegetation type zones in arid zones, was conducted, revealing the response mechanisms of different plant organ growth to climate change. We found that the climate of the Irtysh River basin trended towards warming and humidification between 1982 and 2015, and plants growth showed significant spatial heterogeneity in response to climate. With increasing altitude, the main climatic limiting factor for the canopy shifts from moisture to temperature. The accumulation of temperature and moisture from early spring and late autumn leads to an earlier and longer growing season, which together promotes the canopy growth. The sensitivity of the plant trunk to climate response decreases with increasing altitude, and the trunk shows a significant correlation with climate only within desert areas. Monthly scale data show that trunk growth is mainly limited by May–June moisture in desert areas, by April–June temperatures and June–August moisture in valley areas, and by April moisture and July temperatures in alpine areas. Canopy growth responds significantly to climate change in the current month, while there is a 1–2-month lag in the response of the trunk to climate. In addition, the syn-

ergy between the canopy and trunk gradually weakens with increasing altitude (correlation coefficient is 0.371 in alpine areas, 0.413 in valley areas and 0.583 in desert areas). Climate change will preferentially disturb the canopy growth, but the impact on trunk growth is inconsistent and needs to be highlighted in the development of climate change response strategies and carbon sink calculations.

Author Contributions: K.Y.: Conceptualization, Data curation, Investigation, Writing—original draft. H.X.: Conceptualization, Methodology, Project administration. G.Z.: Data curation, Investigation. All authors have read and agreed to the published version of the manuscript.

Funding: This research received no external funding.

Acknowledgments: We would like to thank the Xinjiang Institute of Ecology and Geography, Chinese Academy of Sciences for the support of the laboratory work.

Conflicts of Interest: The authors declare that the research was conducted in the absence of any commercial or financial relationships that could be construed as a potential conflict of interest.

References

1. Zheng, K.; Zhou, W.J.; Ying, P.J.; Cheng, H.; Zhang, X.L.; Huang, F.Q.; Li, F.M.; Ye, J.S. Impacts of climate change and human activities on grassland vegetation variation in the Chinese Loess Plateau. *Sci. Total Environ.* **2019**, *660*, 236–244. [CrossRef]
2. Wang, J.; Wang, K.; Zhang, M.; Zhang, C. Impacts of climate change and human activities on vegetation cover in hilly southern China. *Ecol. Eng.* **2015**, *81*, 451–461. [CrossRef]
3. Chen, T.; Tang, G.; Yuan, Y.; Guo, H.; Chen, X. Unraveling the relative impacts of climate change and human activities on grassland productivity in Central Asia over last three decades. *Sci. Total Environ.* **2020**, *743*, 140649. [CrossRef]
4. Li, X.; Li, Y.; Chen, A.; Gao, M.; Slette, I.J.; Piao, S. The impact of the 2009/2010 drought on vegetation growth and terrestrial carbon balance in Southwest China. *Agric. For. Meteorol.* **2019**, *269*, 239–248. [CrossRef]
5. Wu, D.; Piao, S.; Zhu, D.; Wang, X.; Xu, W. Accelerated terrestrial ecosystem carbon turnover and its drivers. *Glob. Change Biol.* **2020**, *26*, 5052–5062. [CrossRef]
6. Gang, C.; Zhang, Y.; Wang, Z.; Chen, Y.; Yang, Y.; Li, J.; Cheng, J.; Qi, J.; Odeh, I. Modeling the dynamics of distribution, extent, and NPP of global terrestrial ecosystems in response to future climate change. *Glob. Planet. Change* **2017**, *148*, 153–165. [CrossRef]
7. Jiang, W.; Yuan, L.; Wang, W.; Cao, R.; Zhang, Y.; Shen, W. Spatio-temporal analysis of vegetation variation in the yellow river basin. *Ecol. Indic.* **2015**, *51*, 117–126. [CrossRef]
8. Maclean, L.M.D.; Wilson, R.J. Recent ecological responses to climate change support predictions of high extinction risk. *Proc. Natl. Acad. Sci. USA* **2011**, *108*, 12337–12342. [CrossRef]
9. Berdugo, M.; Delgado-Baquerizo, M.; Soliveres, S.; Hernández-Clemente, R.; Zhao, Y.C.; Gaitán, J.J.; Gross, N.; Saiz, H.; Maire, V.; Lehmann, A.; et al. Global ecosystem thresholds driven by aridity. *Science* **2020**, *367*, 787–790. [CrossRef]
10. Erb, K.H.; Kastner, T.; Plutzar, C.; Bais, A.L.S.; Carvalhais, N.; Fetzel, T.; Gingrich, S.; Haberl, H.; Lauk, C.; Niedertscheider, M.; et al. Unexpectedly large impact of forest management and grazing on global vegetation biomass. *Nature* **2018**, *553*, 73–76. [CrossRef]
11. Chu, H.; Venevsky, S.; Chao, W.; Wang, M. NDVI-based vegetation dynamics and its response to climate changes at Amur-Heilongjiang River Basin from 1982 to 2015. *Sci. Total Environ.* **2018**, *650 Pt 2*, 2051–2062. [CrossRef] [PubMed]
12. Ammer, C. Diversity and forest productivity in a changing climate. *New Phytol.* **2019**, *221*, 50–66. [CrossRef] [PubMed]
13. Knapp, A.K.; Ciais, P.; Smith, M.D. Reconciling inconsistencies in precipitation—Productivity relationships: Implications for climate change. *New Phytol.* **2016**, *214*, 41–47. [CrossRef] [PubMed]
14. Kawabata, A.; Ichii, K.; Yamaguchi, Y. Global monitoring of interannual changes in vegetation activities using ndvi and its relationships to temperature and precipitation. *Int. J. Remote Sens.* **2001**, *22*, 1377–1382. [CrossRef]
15. Zheng, Y.; Zhang, L.; Zhou, Y.; Zhang, B.H. Vegetation change and its driving factors in global drylands during the period of 1982–2012. *Arid. Zone Res.* **2017**, *34*, 59–66. (In Chinese)
16. Prăvălie, R. Drylands extent and environmental issues. A global approach. *Earth-Sci. Rev.* **2016**, *161*, 259–278. [CrossRef]
17. Li, C.F.; Zhang, C.; Luo, G.P.; Chen, X. Modeling the carbon dynamics of the dryland ecosystems in Xinjiang, China from 1981 to 2007—The spatiotemporal patterns and climate controls. *Ecol. Model.* **2013**, *267*, 148–157. [CrossRef]
18. Li, C.; Zhang, C.; Luo, G.P.; Chen, X.; Maisupova, B.; Madaminov, A.A.; Han, Q.; Djenbaev, B.M. Carbon stock and its responses to climate change in Central Asia. *Glob. Change Biol.* **2015**, *21*, 1951–1967. [CrossRef]
19. Huang, J.; Yu, H.; Dai, A.; Wei, Y.; Kang, L. Drylands face potential threat under 2 °C global warming target. *Nat. Clim. Change* **2017**, *7*, 417–422. [CrossRef]
20. Abbott, B.W.; Bishop, K.; Zarnetske, J.P.; Minaudo, C.; Pinay, G. Human domination of the global water cycle absent from depictions and perceptions. *Nat. Geosci.* **2019**, *12*, 533–540. [CrossRef]
21. Hamann, E.; Denney, D.; Day, S.; Lombardi, E.; Jameel, M.I.; MacTavish, R.; Anderson, J.T. Review: Plant eco-evolutionary responses to climate change: Emerging directions. *Plant Sci.* **2020**, *304*, 110737. [CrossRef] [PubMed]

22. Zellweger, F.; Frenne, P.D.; Lenoir, J.; Vangansbeke, P.; Verheyen, K.; Bernhardt-Römermann, M.; Baeten, L.; Hédl, R.; Berki, I.; Brunet, J.; et al. Forest microclimate dynamics drive plant responses to warming. *Science* **2020**, *368*, 772–775. [CrossRef] [PubMed]
23. Ge, W.; Deng, L.; Wang, F.; Han, J. Quantifying the contributions of human activities and climate change to vegetation net primary productivity dynamics in China from 2001 to 2016. *Sci. Total Environ.* **2021**, *773*, 145648. [CrossRef] [PubMed]
24. Zhou, Y.; Yi, Y.J.; Jia, W.F.; Cai, Y.; Li, Z. Applying dendrochronology and remote sensing to explore climate-drive in montane forests over space and time. *Quat. Sci. Rev.* **2020**, *237*, 106292. [CrossRef]
25. Reichstein, M.; Bahn, M.; Ciais, P.; Frank, D.; Mahecha, M.D.; Seneviratne, S.I.; Zscheischler, J.; Beer, C.; Buchmann, N.; Frank, D.C. Climate extremes and the carbon cycle. *Nature* **2013**, *500*, 287–295. [CrossRef] [PubMed]
26. Kannenberg, S.A.; Novick, K.A.; Alexander, M.R.; Maxwell, J.T.; Moore, D.J.P.; Phillips, R.P.; Anderegg, W.R.L. Linking drought legacy effects across scales: From leaves to tree rings to ecosystems. *Glob. Change Biol.* **2019**, *25*, 2978–2992. [CrossRef]
27. Chen, F.; Yuan, Y.J.; Zhang, R.B.; Yu, S.L. Reconstruction of Regional NDVI Using Tree-ring Width Chronology in the Southern Edge of the Badain Jaran Desert, Northwestern China. *Desert Oasis Meteorol.* **2015**, *9*, 1033–1044.
28. Wu, Q.Q.; Zhang, X.; Xu, S.X.; Yang, X.H.; Liu, Y.S.; Zhang, H.Z.; Shi, Z.J. Climatic responses of NDVI and tree growth in the arid areas of inland Asia and their influencing factors. *J. Desert Res.* **2022**, *42*, 1–10. (In Chinese)
29. Cao, R.Y.; Chen, Y.; Shen, M.G.; Chen, J.; Zhou, J.; Wang, C.; Yang, W. A simple method to improve the quality of NDVI time-series data by integrating spatiotemporal information with the Savitzky-Golay filter. *Remote Sens. Environ.* **2018**, *217*, 244–257. [CrossRef]
30. Bigler, C.; Grahn, E.; Laroque, I.; Jeziorski, A.; Hall, R. Holocene environmental change at Lake Njulla (999 m a.s.l.), northern Sweden:a comparison with four small nearby lakes along an altitudinal Gradient. *J. Paleolimnol.* **2003**, *29*, 13–29. [CrossRef]
31. Grissino-Mayer, H. Evaluating cross-dating accuracy: A manual and tutorial for the computer program COFECHA. *Tree-Ring Res.* **2001**, *57*, 205–221.
32. Cook, E.R. *A Time-Series Analysis Approach to Tree-Ring Standardization*; University of Arizona: Tucson, AZ, USA, 1985.
33. Fritts, H.C. *Tree Ring and Climate*; Academic Press: London, UK, 1976.
34. Vicente-Serrano, S.M.; Beguería, S.; Lopez-Moreno, J.I. A multiscalar drought index sensitive to global warming: The standardized precipitation evapotranspiration index. *J. Clim.* **2010**, *23*, 1696–1718. [CrossRef]
35. Vicente-Serrano, S.M.; Gouveia, C.; Camarero, J.J.; Begueria, S.; Trigo, R.; Lopez-Moreno, J.I.; Azorín-Molina, C.; Pasho, E.; Lorenzo-Lacruz, J.; Revuelto, J.; et al. Response of vegetation to drought time-scales across global land biomes. *Proc. Natl. Acad. Sci. USA* **2013**, *110*, 52–57. [CrossRef] [PubMed]
36. Kendall, M.G. Rank correlation methods. *Br. J.* **1990**, *25*, 86–91. [CrossRef]
37. Mann, H.B. Non-parametric test against trend. *Econometrica* **1945**, *13*, 245–259. [CrossRef]
38. Attaur, R.; Dawood, M. Spatio-statistical analysis of temperature fluctuation using Mann-Kendall and Sen's slope approach. *Clim. Dyn.* **2017**, *48*, 783–797.
39. Coen, M.C.; Andrews, E.; Bigi, A.; Martucci, G.; Romanens, G.; Vogt, F.P.A.; Vuilleumier, L. Effects of the prewhitening method, the time granularity, and the time segmentation on the Mann-Kendall trend detection and the associated Sen's slope. *Atmos. Meas. Tech.* **2020**, *13*, 6945–6964. [CrossRef]
40. Ma, X.F.; Yan, W.; Zhao, C.Y.; Kundzewicz, Z.W. Snow-cover area and runoff variation under climate change in the West Kunlun Mountains. *Water* **2019**, *11*, 2246. [CrossRef]
41. Prislan, P.; Gricar, J.; De, L.M.; Smith, K.T.; Cufar, K. Phenological variation in xylem and phloem formation in *Fagus sylvatica* from two contrasting sites. *Agric. For. Meteorol.* **2013**, *180*, 142–151. [CrossRef]
42. Ren, S.; An, S. Temporal Pattern Analysis of Cropland Phenology in Shandong Province of China Based on Two Long-Sequence Remote Sensing Data. *Remote Sens.* **2021**, *13*, 4071. [CrossRef]
43. Xin, Q.C.; Broich, M.; Zhu, P.; Gong, P. Modeling grassland spring onset across the Western United States using climate variables and MODIS—Derived phenology metrics. *Remote Sens. Environ.* **2015**, *161*, 63–77. [CrossRef]
44. Miao, L.; Daniel, M.; Cui, X.; Ma, M.; Sylvain, D. Changes in vegetation phenology on the Mongolian Plateau and their climatic determinants. *PLoS ONE* **2017**, *12*, e0190313. [CrossRef] [PubMed]
45. Lian, X.; Piao, S.; Li, L.Z.X.; Li, Y.; He, G. Summer soil drying exacerbated by earlier spring greening of northern vegetation. *Sci. Adv.* **2020**, *6*, eaax0255. [CrossRef] [PubMed]
46. Yang, Y.; Guan, H.; Shen, M.; Liang, W.; Jiang, L. Changes in autumn vegetation dormancy onset date and the climate controls across temperate ecosystems in China from 1982 to 2010. *Glob. Change Biol.* **2015**, *21*, 652–665. [CrossRef] [PubMed]
47. Altman, J.; Fibich, P.; Santruckova, H.; Dolezal, J.; Stepanek, P.; Kopacek, J.; Hunova, L.; Oulehle, F.; Tumajer, J.; Cienciala, E. Environmental factors exert strong control over the climate-growth relationships of Picea abies in Central Europe. *Sci. Total Environ.* **2017**, *609*, 506–516. [CrossRef] [PubMed]
48. Gao, M.; Piao, S.; Chen, A.; Yang, H.; Liu, Q.; Fu, Y.; Janssens, I. Divergent changes in the elevational gradient of vegetation activities over the last 30 years. *Nat. Commun.* **2019**, *10*, 2970. [CrossRef] [PubMed]
49. Li, Z.; Li, X.; Rubert-Nason, K.F.; Yang, Q.; Fu, Q.; Feng, J.; Shi, S. Photosynthetic acclimation of an evergreen broadleaved shrub (*Ammopiptanthus mongolicus*) to seasonal climate extremes on the Alxa Plateau, a cold desert ecosystem. *Trees* **2018**, *32*, 603–614. [CrossRef]
50. Aikio, S.; Taulavuori, K.; Hurskainen, S.; Taulavuori, E.; Tuomi, J.; Mäkelä, A. Contributions of day length, temperature and individual variability on the rate and timing of leaf senescence in the common lilac Syringa vulgaris. *Tree Physiol.* **2019**, *39*, 961–970. [CrossRef]

51. Jeong, S.J.; Ho, C.H.; Park, T.W.; Kim, J.; Levis, S. Impact of vegetation feedback on the temperature and its diurnal range over the Northern Hemisphere during summer in a 2 × CO_2 climate. *Clim. Dyn.* **2011**, *37*, 821–833. [CrossRef]
52. Vetaas, O.R.; Paudel, K.P.; Christensen, M. Principal factors controlling biodiversity along an elevation gradient: Water, energy and their interaction. *J. Biogeogr.* **2019**, *46*, 1652–1663. [CrossRef]
53. Myers-Smith, I.H.; Kerby, J.T.; Phoenix, G.K.; Bjerke, J.W.; Epstein, H.E.; Assmann, J.J.; John, C.; Andreu-Hayles, L.; Angers-Blondin, S.; Beck, P.S.A.; et al. Complexity revealed in the greening of the Arctic. *Nat. Clim. Change* **2020**, *10*, 106–117. [CrossRef]
54. Wang, S.; Wang, C.; Duan, J.; Zhu, X.; Du, M. Timing and duration of phenological sequences of alpine plants along an elevation gradient on the Tibetan plateau. *Agric. For. Meteorol.* **2014**, *189–190*, 220–228. [CrossRef]
55. Xie, J.; Kneubühler, M.; Garonna, I.; Notarnicola, C.; Schaepman, M.E. Altitude-dependent influence of snow cover on alpine land surface phenology. *J. Geophys. Res.* **2017**, *122*, 1107–1122. [CrossRef]
56. Deng, C.; Bai, H.; Gao, S.; Zhao, T.; Ma, X. Differences and variations in the elevation-dependent climatic growing season of the northern and southern slopes of the Qinling Mountains of China from 1985 to 2015. *Theor. Appl. Climatol.* **2018**, *137*, 1159–1169. [CrossRef]
57. Zhu, W.; Zhang, X.; Zhang, J.; Zhu, L. A comprehensive analysis of phenological changes in forest vegetation of the Funiu Mountains, China. *J. Geogr. Sci.* **2019**, *29*, 131–145. [CrossRef]
58. Liu, H.; Park, W.A.; Allen, C.D.; Guo, D.; Wu, X.; Anenkhonov, O.A.; Liang, E.; Sandanov, D.V.; Yin, Y.; Qi, Z.; et al. Rapid warming accelerates tree growth decline in semi-arid forests of Inner Asia. *Glob. Change Biol.* **2013**, *19*, 2500–2510. [CrossRef]
59. Mishra, N.B.; Mainali, K.P. Greening and browning of the Himalaya: Spatial patterns and the role of climatic change and human drivers. *Sci. Total Environ.* **2017**, *587–588*, 326–339. [CrossRef]
60. Wu, D.; Zhao, X.; Liang, S.; Zhou, T.; Huang, K.; Tang, B.; Zhao, W. Time-lag effects of global vegetation responses to climate change. *Glob. Change Biol.* **2015**, *21*, 3520–3531. [CrossRef]
61. Rossi, S.; Anfodillo, T.; Cufar, K.; Cuny, H.E.; Deslauriers, A.; Fonti, P.; Frank, D.; Gričar, J.; Gruber, A.; Huang, J.G.; et al. Pattern of xylem phenology in conifers of cold ecosystems at the Northern Hemisphere. *Glob. Change Biol.* **2016**, *22*, 3804–3813. [CrossRef]
62. Smith, B.; Wårlind, D.; Arneth, A.; Hickler, T.; Leadley, P.; Siltberg, J.; Zaehle, S. Implications of incorporating N cycling and N limitations on primary production in an individual-based dynamic vegetation model. *Biogeosciences* **2014**, *11*, 2027–2054. [CrossRef]
63. Gou, X.H.; Chen, F.H.; Yang, M.X.; Peng, J.F.; Chen, T. Analysis of the tree-ring width chronology of Qilian Mountains at different elevation. *Acta Ecol. Sin.* **2004**, *24*, 172–176. (In Chinese)
64. Liu, L.S.; Shao, X.M.; Liang, E.Y. Climate signals from tree ring chronologies of the upper and lower treelines in the Dulan region of the Northeastern Qinghai—Tibetan Plateau. *J. Integr. Plant Biol.* **2006**, *48*, 278–285. [CrossRef]
65. Peng, J.F.; Gou, X.H.; Chen, F.H.; Liu, P.X.; Zhang, Y. Characteristics of ring width chronologies of *Picea crassifolia* and their responses to climate at different elevations in the Anyemaqen Mountains. *Acta Ecol. Sin.* **2007**, *27*, 3268–3276. (In Chinese)
66. Qiang, W.Y.; Wang, X.L.; Chen, T.; Feng, H.Y.; An, L.Z.; He, Y.Q.; Wang, G. Variations of stomatal density and carbon isotope values of Picea crassifolia at different altitudes in the Qilian Mountains. *Trees* **2003**, *17*, 258–262. [CrossRef]
67. Seftigen, K.; Frank, D.C.; Björklund, J.; Babst, F.; Poulter, B. The climatic drivers of normalized difference vegetation index and tree-ring-based estimates of forest productivity are spatially coherent but temporally decoupled in Northern Hemispheric forests. *Glob. Ecol. Biogeogr.* **2018**, *27*, 1352–1365. [CrossRef]
68. Camarero, J.J.; Rozas, V.; Olano, J.M. Minimum wood density of Juniperus thurifera is a robust proxy of spring water availability in a continental Mediterranean climate. *J. Biogeogr.* **2014**, *41*, 1105–1114. [CrossRef]
69. Deslauriers, A.; Huang, J.G.; Balducci, L.; Beaulieu, M.; Rossi, S. The contribution of carbon and water in modulating wood formation in black spruce saplings. *Plant Physiol.* **2016**, *170*, 2072–2084. [CrossRef]
70. Björklund, J.; von Arx, G.; Nievergelt, D.; Wilson, J.; Bulcke, J.V.D.; Günther, B.; Loader, N.J.; Rydval, M.; Fonti, P.; Scharnweber, T.; et al. Scientific merits and analytical challenges of tree-ring densitometry. *Rev. Geophys.* **2019**, *57*, 1224–1264. [CrossRef]
71. Zhou, P.; Huang, J.G.; Liang, H.; Rossi, S.; Bergeron, Y.; Shishov, V.V.; Jiang, S.; Kang, J.; Zhu, H.; Dong, Z. Radial growth of *Larix sibirica* was more sensitive to climate at low than high altitudes in the Altai Mountains, China. *Agric. For. Meteorol.* **2021**, *304–305*, 108392. [CrossRef]
72. Churakova, O.V.; Fonti, M.V.; Saurer, M.; Guillet, S.; Corona, C.; Fonti, P.; Myglan, V.S.; Kirdyanov, A.V.; Naumova, O.V.; Ovchinnikov, D.V.; et al. Siberian tree—Ring and stable isotope proxies as indicators of temperature and moisture changes after major stratospheric volcanic eruptions. *Clim. Past* **2019**, *15*, 685–700. [CrossRef]
73. Björklund, J.; Seftigen, K.; Fonti, P.; Nievergelt, D.; Arx, G.V. Dendroclimatic potential of dendroanatomy in temperature-sensitive Pinus sylvestris. *Dendrochronologia* **2020**, *60*, 125673. [CrossRef]
74. Chang, S.Q. *Preliminary Study on Moisture Sources and Physical Mechanism of Extreme Precipitation Events in the Arid Central Asia*; Lanzhou University: Lanzhou, China, 2019.
75. Bai, X.; Zhang, X.; Li, J.; Duan, X.; Jin, Y.; Chen, Z. Altitudinal disparity in growth of Dahurian larch (*Larix gmelinii Rupr.*) in response to recent climate change in northeast China. *Sci. Total Environ.* **2019**, *670*, 466–477. [CrossRef] [PubMed]
76. Niu, X.D.; Jiang, H.; Zhang, J.M.; Fang, C.Y.; Sun, H. Characteristics of CO_2 flux in an old growth mixed forest in Tianmu Mountain, Zhejiang, China. *Chin. J. Appl. Ecol.* **2016**, *27*, 1–8. (In Chinese)

77. Wang, Q.; Wang, Y.Q.; Chao, M.; Wang, B.; Li, Y.F. Characteristics of carbon fluxes and their response to environmental factors in ecosystems of mixed coniferous and broad-leaved forests in Jinyun Mountain. *Resour. Environ. Yangtze Basin* **2019**, *28*, 75–86. (In Chinese)
78. Zhang, X.W.; Liu, X.H.; Zhang, Q.L.; Zeng, X.M.; Xu, G.B.; Wu, G.J.; Wang, W.Z. Species-specific tree growth and intrinsic water—Use efficiency of Dahurian larch (*Larix gmelinii*) and Mongolian pine (*Pinus sylvestris* var. *mongolica*) growing in a boreal permafrost region of the Greater Hinggan Mountains, Northeastern China. *Agric. For. Meteorol.* **2018**, *248*, 145–155. [CrossRef]
79. Malyshev, A.V. Warming events advance or delay spring phenology by affecting bud dormancy depth in trees. *Front. Plant Sci.* **2020**, *11*, 856. [CrossRef]
80. Ma, Q.Q.; Huang, J.G.; Hänninen, H.; Berninger, F. Divergent trends in the risk of spring frost damage to trees in Europe with recent warming. *Glob. Change Biol.* **2018**, *25*, 351–360. [CrossRef]
81. Jiang, S.; Liang, H.; Zhou, P.; Wang, Z.; Huang, J.G. Spatial and temporal differences in the response of *Larix sibirica* to climate change in the central Altai Mountains. *Dendrochronologia* **2021**, *3*, 125827. [CrossRef]
82. Baumbach, L.; Siegmund, J.F.; Mittermeier, M.; Donner, R.V. Impacts of temperature extremes on European vegetation during the growing season. *Biogeosciences* **2017**, *14*, 4891–4903. [CrossRef]
83. Vicente-Serrano, S.M.; Martín-Hernández, N.; Camarero, J.J.; Gazol, A.; Sánchez-Salguero, R.; Peña-Gallardo, M.; Kenawy, A.E.; Domínguez-Castro, F.; Tomas-Burguera, M.; Gutiérrez, E.; et al. Linking tree—Ring growth and satellite-derived gross primary growth in multiple forest biomes. Temporal-scale matters. *Ecol. Indic.* **2020**, *108*, 105753. [CrossRef]
84. Alla, A.Q.; Pasho, E.; Marku, V. Growth variability and contrasting climatic responses of two Quercus macrolepis stands from Southern Albania. *Trees* **2017**, *31*, 1491–1504. [CrossRef]
85. Coulthard, B.L.; Touchan, R.; Anchukaitis, K.J.; Meko, D.M.; Sivrikaya, F. Tree growth and vegetation activity at the ecosystem-scale in the eastern Mediterranean. *Environ. Res. Lett.* **2017**, *12*, 084008. [CrossRef]
86. Sulla-Menashe, D.; Woodcock, C.E.; Friedl, M.A. Canadian boreal forest greening and browning trends: An analysis of biogeographic patterns and the relative roles of disturbance versus climate drivers. *Environ. Res. Lett.* **2018**, *13*, 014007. [CrossRef]
87. Guay, K.C.; Beck, P.S.A.; Berner, L.T.; Goetz, S.J.; Baccini, A. Vegetation productivity patterns at high northern latitudes: A multi-sensor satellite data assessment. *Glob. Change Biol.* **2014**, *20*, 3147–3158. [CrossRef] [PubMed]
88. Lawley, V.; Lewis, M.; Clarke, K.; Ostendorf, B. Site-based and remote sensing methods for monitoring indicators of vegetation condition:an Australian review. *Ecol. Indic.* **2016**, *60*, 1273–1283. [CrossRef]
89. Zhang, Q.; Kong, D.; Singh, V.P.; Shi, P. Response of vegetation to different time-scales drought across China: Spatiotemporal patterns, causes and implications. *Glob. Planet. Change* **2017**, *152*, 1–11. [CrossRef]
90. Cook, E.R.; Seager, R.; Kushnir, Y.; Briffa, K.R.; Büntgen, U.; Frank, D.; Krusic, P.J.; Tegel, W.; Schrier, G.V.D.; Andreu-Hayles, L.; et al. Old World mega-droughts and pluvials during the Common Era. *Sci. Adv.* **2015**, *1*, e1500561. [CrossRef]
91. Büntgen, U.; Myglan, V.S.; Ljungqvist, F.C.; McCormick, M.; Cosmo, N.D.; Sigl, M.; Jungclaus, J.; Wagner, S.; Krusic, P.J.; Esper, J.; et al. Cooling and societal change during the Late Antique Little Ice Age from 536 to around 660 AD. *Nat. Geosci.* **2016**, *9*, 231–236. [CrossRef]
92. Gauthier, S.; Bernier, P.; Kuuluvainen, T.; Shvidenko, A.Z.; Schepaschenko, D.G. Boreal forest health and global change. *Science* **2015**, *349*, 819–822. [CrossRef]
93. Galiano, L.; Timofeeva, G.; Saurer, M.; Siegwolf, R.; Martínez-Vilalta, J.; Hommel, R.; Gessler, A. The fate of recently fixed carbon after drought release: Towards unravelling C storage regulation in *Tilia platyphyllos* and *Pinus sylvestris*. *Plant Cell Environ.* **2017**, *40*, 1711–1724. [CrossRef]
94. Mitchell, P.J.; O'Grady, A.P.; Tissue, D.T.; Worledge, D.; Pinkard, E.A. Co-ordination of growth, gas exchange and hydraulics define the carbon safety margin in tree species with contrasting drought strategies. *Tree Physiol.* **2014**, *34*, 443–458. [CrossRef]
95. Sala, A.; Woodruff, D.R.; Meinzer, F.C. Carbon dynamics in trees: Feast or famine? *Tree Physiol.* **2012**, *32*, 764–775. [CrossRef]
96. Kannenberg, S.A.; Schwalm, C.R.; Anderegg, W.R. Ghosts of the past: How drought legacy effects shape forest functioning and carbon cycling. *Ecol. Lett.* **2020**, *23*, 891–901. [CrossRef]
97. Gough, C.M.; Vogel, C.S.; Schmid, H.P.; Su, H.B.; Curtis, P.S. Multi-year convergence of biometric and meteorological estimates of forest carbon storage. *Agric. For. Meteorol.* **2008**, *148*, 158–170. [CrossRef]
98. Cuny, H.E.; Rathgeber, C.B.K.; Frank, D.; Fonti, P.; Makinen, H.; Prislan, P.; Rossi, S.; Castillo, E.M.d.; Campelo, F.; Vavrčík, H.; et al. Woody biomass production lags stem-girth increase by over one month in coniferous forests. *Nat. Plants* **2015**, *1*, 15160. [CrossRef]
99. Cai, Q.; Liu, Y. Two centuries temperature variations over subtropical southeast China inferred from *Pinus taiwanensis* Hayata tree-ring width. *Clim. Dyn.* **2017**, *48*, 1813–1825. [CrossRef]
100. Shi, Z.J.; Xu, L.H.; Dong, L.S.; Gao, J.X.; Yang, X.H.; Lü, S.H.; Feng, C.Y.; Shang, J.X.; Song, A.Y.; Guo, H.; et al. Growth-climate response and drought reconstruction from tree-ring of Mongolian pine in Hulunbuir, Northeast China. *J. Plant Ecol.* **2016**, *9*, 51–60. [CrossRef]
101. Ruibo, Z. *Tree-Ring-Based Droughts Variability in Western Tianshan Mountains, Central Asia*; College of Earth and Environment Sciences: Lanzhou, China, 2017.